(2)

Technical Report 1372
February 1991

Thickness Measurements of Silicon Films Using Partial Coherence Interferometry

M. N. McLandrich
D. J. Albares

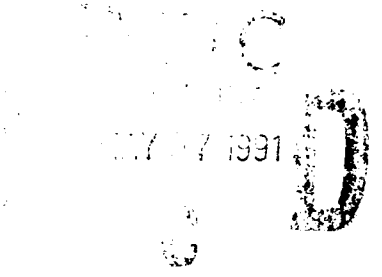

NAVAL OCEAN SYSTEMS CENTER

San Diego, California 92152–5000

J. D. FONTANA, CAPT, USN
Commander

H. R. TALKINGTON, Acting
Technical Director

ADMINISTRATIVE INFORMATION

This work was performed for the Strategic Systems Project Office, Washington, DC 20360, under program element WPN. Work was performed by members of Codes 555 and 553, NOSC.

Released by
M. N. McLandrich, Head
Optical Electronics Branch

Under authority of
H. E. Rast, Head
Electronic Material
Sciences Division

MA

SUMMARY

OBJECTIVE

Determine the feasibility of using an optical system composed of a remote fiber-optic probe coupled to a scanning partial coherence Michelson interferometer for localized thickness measurement of thin silicon films.

RESULTS

A partial coherence interferometer, combined with an optical fiber coupler probe has been designed, assembled, characterized, and used to accurately measure the thickness of a thin silicon substrate charge-coupled device (CCD). The system has been configured in a way that it can be adapted to measure thick samples, and to perform in situ measurements of samples during the etching process. Feasibility of the measurement technique has been demonstrated on actual processed CCD devices with a nominal thickness of 8 μm, and an estimated precision of 1.3 percent, or 0.1 μm, has been achieved.

CONCLUSIONS AND RECOMMENDATIONS

A remote fiber-optic probe coupled to a scanning Michelson interferometer can be configured into an optical system to perform in situ precision measurements of thin silicon film thickness.

Such a system can function in realtime during a manufacturing process, such as film deposition or removal, and can be used to aid in the control of the process.

The prototype laboratory model developed in this program should be modified to demonstrate this capability and assess its limitations.

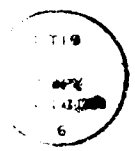

CONTENTS

INTRODUCTION 1

PARTIAL COHERENCE INTERFEROMETRY 1

EXPERIMENTAL CONFIGURATION 6

MEASUREMENT METHODOLOGY 7

EXPERIMENTAL RESULTS 10

DISCUSSION AND CONCLUSIONS 12

REFERENCES 15

GLOSSARY OF SYMBOLS AND ABBREVIATIONS 16

APPENDIX A—THEORETICAL DERIVATION OF THE INTERFEROGRAM FOR A SYMMETRIC MICHELSON INTERFEROMETER WITH A TWO-BEAM INPUT FROM A DISPERSIVE MEDIUM A-1

FIGURES

1. Optical source spectral energy distribution and wave packet emission representation of source output. Coherence length l_c of source is determined by spectral width $\delta\lambda$ 2

2. Recombination of amplitude-divided wave packet from source.
   (a) Path difference between waves $\Delta p > l_c$
   (b) Path difference $\Delta p \lesssim l_c$ 2

3. Source interferogram calculated for a Gaussian spectral distribution source. Assumed parameters are $\lambda_o = 830$ nm and $\delta\lambda = 60$ nm 4

4. Spectral distributions for (a) a pure Gaussian source, (b) a Gaussian with periodic structure superimposed, and (c) a Gaussian with asymmetric periodic structure superimposed 5

5. Source interferograms calculated for the source spectral distributions in figure 4 5

6. Experimental configuration for the measurement of CCD sample film thickness using an optical fiber coupler probe, a Michelson interferometer, and a partially coherent source 6

7. Relative delay of front-surface- and back-surface-reflected wave packets from sample by means of Michelson interferometer variable piezoelectric transducer displacement p_t 7

8. Computer-generated sample interferogram. Assumed values are $\lambda_o = 0.83$ μm, $\delta\lambda = 25$ nm, and $t = 7.5$ μm 8

9. Spectral distribution for ELED used in the experiments at an operating at 10 mA. Mean wavelength is 847 nm and spectral width is approximately 20 nm 10

CONTENTS (Continued)

FIGURES (continued)

10. Actual sample interferogram obtained by photographing oscilloscope recording of detector-amplifier-output voltage versus piezoelectric-transducer-ramp voltage. Number of fringes from central maximum to secondary maximum is N = 79, corresponding to a sample thickness of $t = 7.8$ μm 11

11. ELED source spectra at 25°C for various operating currents. Presence of structure and asymmetry increase as current increases, while mean wavelength shifts to smaller values 13

12. Source interferogram for ELED operating at a current of 10 mA. Minimal periodic structure is indicated by lack of significant interferogram amplitude other than central envelope 14

TABLES

1. Results of sample thickness measurement 11

2. Sample thickness variation with position 12

INTRODUCTION

For a particular Navy application, it is necessary to "thin" the substrate of a silicon charge-coupled device (CCD) after the device sensor array and microcircuitry have been processed. This enables back-plane illumination of the CCD without significant attenuation or scattering of the optical signals incident on the sensor. Thinning is done by means of an etching technique, which must be controlled precisely, and therefore, it is advantageous to be able to measure the substrate thickness during the etching process. Furthermore, the final thickness of the etched silicon substrate must be known precisely, with an accuracy on the order of 0.1 μm.

A partial coherence interferometer, combined with an optical fiber coupler probe has been designed, assembled, characterized, and used to accurately measure the thickness of a thin silicon substrate CCD. The system has been configured in a way that it can be adapted to measure thick samples, and to perform in situ measurements of samples during the etching process. Feasibility of the measurement technique has been demonstrated on actual processed CCD devices with a nominal thickness of 8 μm, and an estimated precision of 1.3 percent, or 0.1 μm has been achieved.

PARTIAL COHERENCE INTERFEROMETRY

Partial coherence exists in an interferometric system whenever the optical source cannot be considered purely monochromatic. That is, it has a spectral distribution with a bandwidth (in wavenumbers) comparable to the inverse of the differential path length of the optical beams propagating in the interferometer. The spectral distribution is characterized by a central wavelength, λ_o, and a spectral bandwidth, $\delta\lambda$, or alternatively, in wavenumbers by $\sigma_o = 1/\lambda_o$ and $\delta\sigma = \delta\lambda/\lambda_o^2$ (see figure 1). The coherence length, l_c, of the source is a measure of the distance over which two beams or wave packets, which are derived from the source by means of amplitude division, will produce high-visibility interference fringes when they are recombined. The expression for l_c in terms of the spectral parameters is[1]

$$l_c = 1/\delta\sigma = \lambda_o^2/\delta\lambda \tag{1}$$

The relationship between source bandwidth, coherence, and fringe visibility is shown schematically in figure 2 where the output from the source is represented by a wave packet of length l_c. The wave packet is divided into two equal amplitude waves, then recombined after traversing optical-path lengths differing by an amount, Δp. (An optical system that can perform this function is a Michelson interferometer described later.) In figure 2a, the waves are assumed to have traveled over optical paths differing by an amount, Δp, which is greater than the coherence length of the source. In this case, there is no longitudinal spatial overlap of the wave packets when they are recombined, and the beams are incoherent with an intensity equal to the sum of the individual wave intensities. If the waves traverse optical paths differing by an amount, $\Delta p < l_c$, then there is longitudinal spatial overlap and the waves are partially coherent when they are recombined. (Complete coherence exists only for $\Delta p = 0$.) In this case, shown in figure 2b, the intensity depends on the phase difference between the waves being proportional to the optical path difference.

As the path difference, Δp, is increased from 0, the intensity will vary in a cosinusoidal way, with a continuously decreasing amplitude. This amplitude factor is a function of l_c and also of Δp, and is known as the fringe visibility[2] or mutual coherence function γ.[3] This function is determined by the spectral distribution of the source, and therefore, source spectral characteristics are a critical factor in the ability to measure sample thickness using Michelson interferometry.

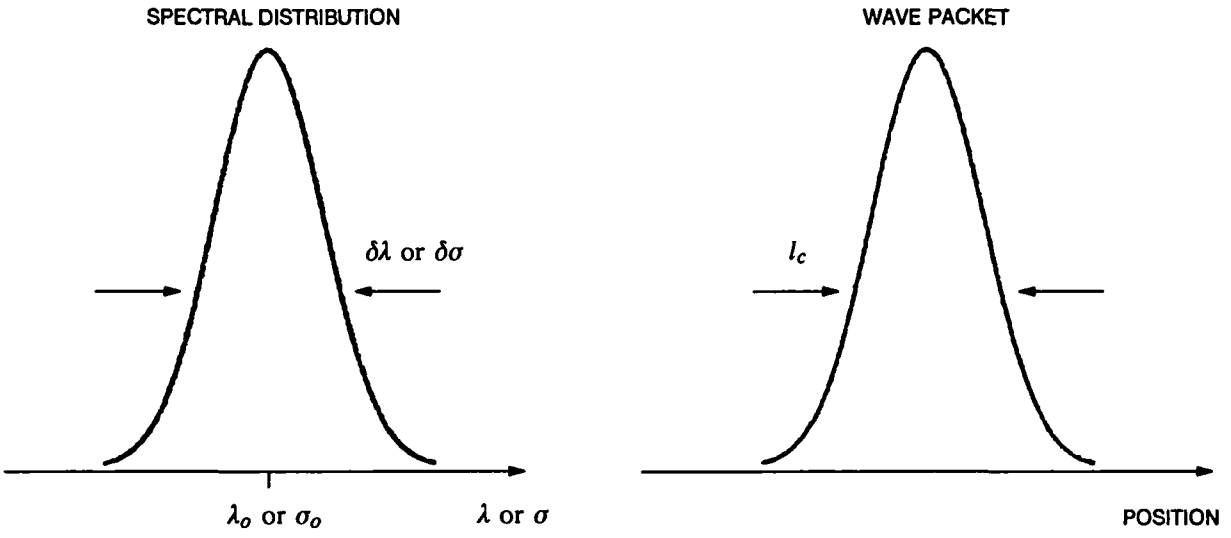

$$l_c = 1/\delta\sigma = \lambda_o^2/\delta\lambda$$

Figure 1. Optical source spectral energy distribution and wave packet emission representation of source output. Coherence length l_c of source is determined by spectral width $\delta\lambda$.

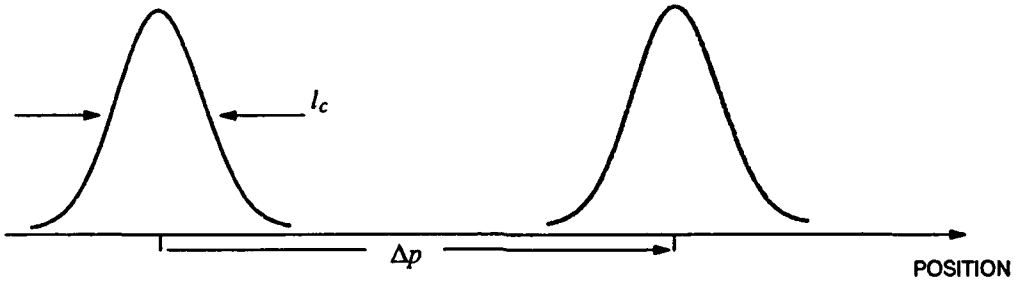

(a) $\Delta p > l_c \quad I(\Delta p) = I_1 + I_2$

(b) $\Delta p < l_c \quad I(\Delta p) = (I_1 + I_2)[1 + \gamma(\Delta p)\cos(2\pi\sigma_o\Delta p)]$

Figure 2. Recombination of amplitude-divided wave packet from source. (a) Path difference between waves $\Delta p > l_c$. (b) Path difference $\Delta p \leq l_c$.

As an example of the interference of waves produced by a source with an extended spectral distribution, the case of a Gaussian distribution is considered here. If the source optical field is represented by the function $E_s(\sigma)$, then the field produced by the interfering beams for a wavenumber component σ at a time, t, is

$$E(\sigma) = Re\{\tfrac{1}{2}E_s(\sigma)(\exp[i(2\pi\sigma p_1 - \omega t)] + \exp[i(2\pi\sigma p_2 - \omega t)])\} \tag{2}$$

where p_1 and p_2 are the optical paths of the two waves. The components of the field are assumed to have the same polarization and that the optical paths are in a nondispersive medium. (The more general case including a dispersive optical path is discussed in Appendix A.) Also assumed are the source can be treated as a point source, and that there is no angular misalignment between the interfering waves. Under these conditions, there is no transverse spatial variation of $E(\sigma)$. The time-averaged intensity for a particular wavenumber component of the source is then given by

$$I(\sigma) = |E(\sigma)|^2 = \tfrac{1}{2}|E_s(\sigma)|^2[1 + \cos(2\pi\sigma\Delta p)] \tag{3}$$

where $\Delta p = p_1 - p_2$. The total intensity is found by integrating the intensities resulting from each component of the source spectrum. The total time-averaged intensity is then given by

$$I_t(\Delta p) = \int I(\sigma)d\sigma = \tfrac{1}{2}\int |E_s(\sigma)|^2 d\sigma + \tfrac{1}{2}\int |E_s(\sigma)|^2 \cos(2\pi\sigma\Delta p)d\sigma \ . \tag{4}$$

The first term above is constant and represents the background intensity level equal to half the source intensity, or equivalently, $I_t(\infty)$. The second term varies with respect to the path difference, Δp, and for nondispersive media it is simply the Fourier cosine transform of the source energy spectral distribution.

For a point source with a normalized Gaussian spectral distribution given by

$$|E_s(\sigma)|^2 = (1/\delta\sigma)\exp\{-\pi[(\sigma - \sigma_o)/\delta\sigma]^2\} \tag{5}$$

the normalized intensity as a function of Δp is from equations (4) and (5)

$$I_t(\Delta p) = \tfrac{1}{2}\{1 + \exp[-\pi(\Delta p\delta\sigma)^2]\cos(2\pi\sigma_o\Delta p)\} \tag{6}$$

From this expression, the general observations made regarding the interference intensity are confirmed. First, in regions of nonzero fringe visibility (i.e., $\Delta p \lesssim 1/\delta\sigma$), the intensity varies as the cosine of a term proportional to the optical-path difference, Δp, and with a period equal to the mean wavelength of the source distribution, $\lambda_o = 1/\sigma_o$. Second, the fringe visibility decreases as the difference in optical-path length, Δp, increases. Also, the extent of the fringe visibility is correlated to the quantity, l_c, the coherence length of the source equal to the inverse of the spectral width of the source $l_c \simeq 1/\delta\sigma$.

Figure 3 is a plot of the variable intensity term in equation (6) as a function of Δp. This type of graph known as the source interferogram can be produced by a scanning Michelson interferometer. The source parameters used in equation 6 to generate this plot are λ_o = 830 nm and $\delta\lambda$ = 60 nm.

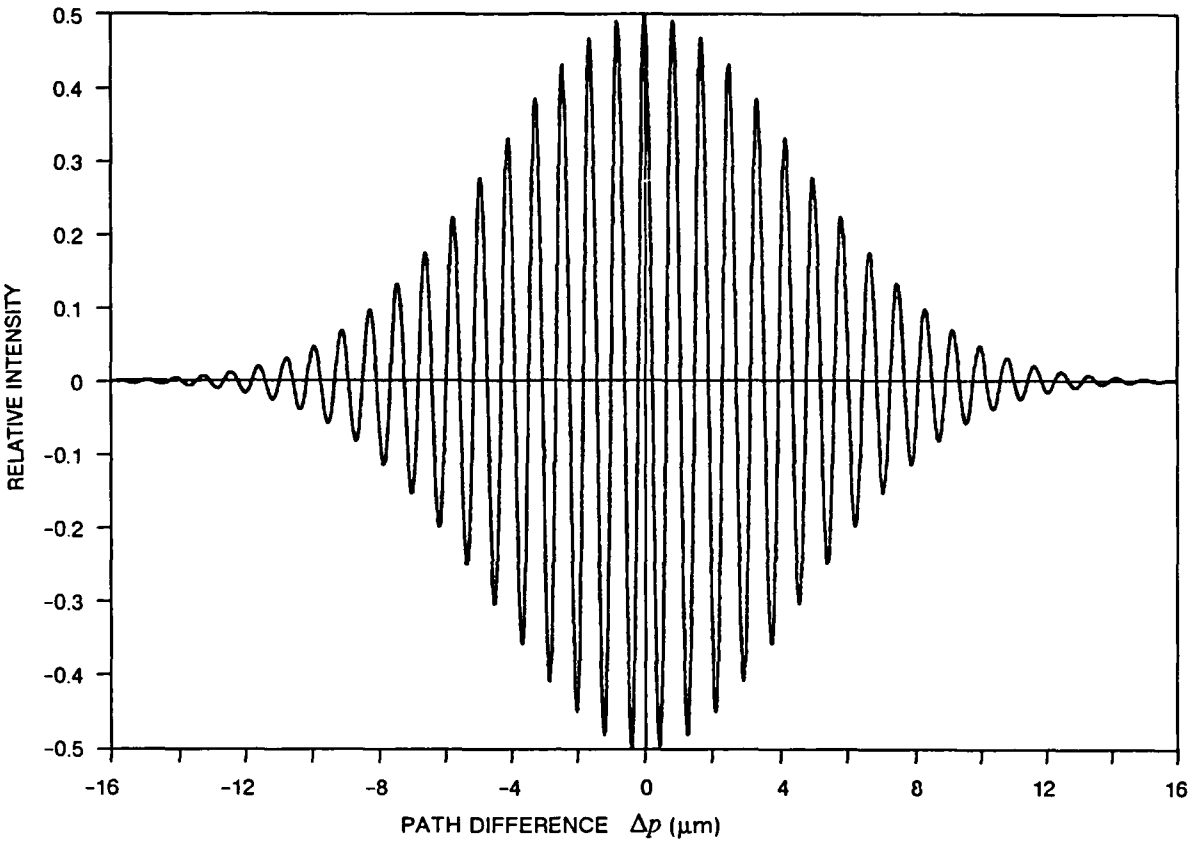

Figure 3. Source interferogram calculated for a Gaussian spectral distribution source. Assumed parameters are λ_o = 830 nm and $\delta\lambda$ = 60 nm.

Although the above statements regarding the features of the interferogram are made for a source with a Gaussian distribution, they are true qualitatively for a general source. In practice, the source is not a true Gaussian, in that, it can exhibit structure and asymmetry in the spectrum. Asymmetry in the spectrum has the effect of extending the width of the visibility function, while periodic structure causes sidelobes of appreciable visibility. These effects are shown in the plots in figures 4 and 5. Three different source-spectral-distribution curves are shown in figure 4: (a) corresponding to a pure Gaussian, (b) Gaussian with symmetric periodic structure superimposed, and (c) Gaussian with asymmetric periodic structure. In both b and c, the structure period is $\Delta\lambda$ = 10 nm, or in wavenumbers, $\Delta\sigma$ = 0.0145 μm^{-1}. Each distribution has the same total spectral width of $\delta\lambda$ = 40 nm and a central wavelength of λ_o = 830 nm. The corresponding source interferograms for positive values of the path difference are shown in figure 5. As seen in 5b, the visibility for the symmetric distribution with periodic structure is significantly increased for values of the path length difference in the region of $1/\Delta\sigma$. This is expected since the interferogram is just the Fourier cosine transform of the spectral distribution. Similar results are evident for the asymmetric case in figure 5c. In addition, observe that the envelopes near 0 and $1/\Delta\sigma$ are broadened due to the asymmetry. Note that in both cases, although the visibility function is modified, the period of the fringes remains at the mean wavelength. These effects of spectral structure and asymmetry must be taken into account when measurements of film thickness are made using partial coherence interferometry. This point is further explored in the discussion section.

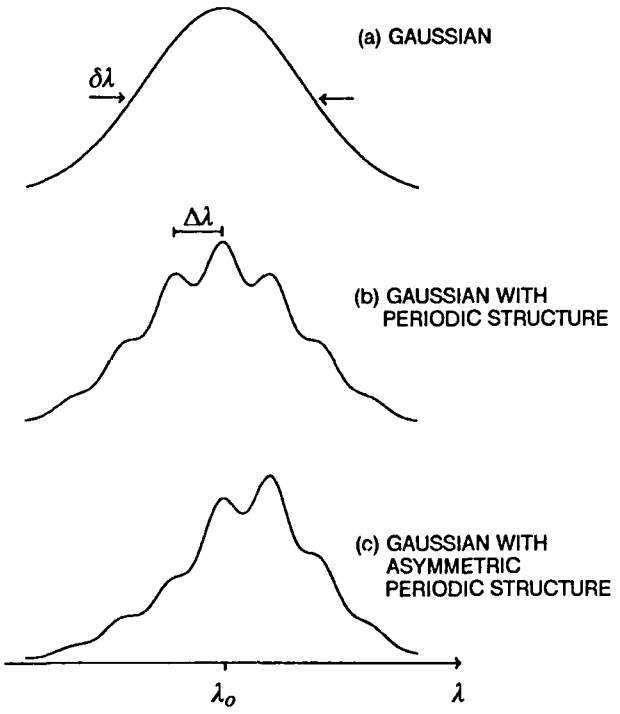

Figure 4. Spectral distributions for (a) a pure Gaussian source, (b) a Gaussian with periodic structure superimposed, and (c) a Gaussian with asymmetric periodic structure superimposed.

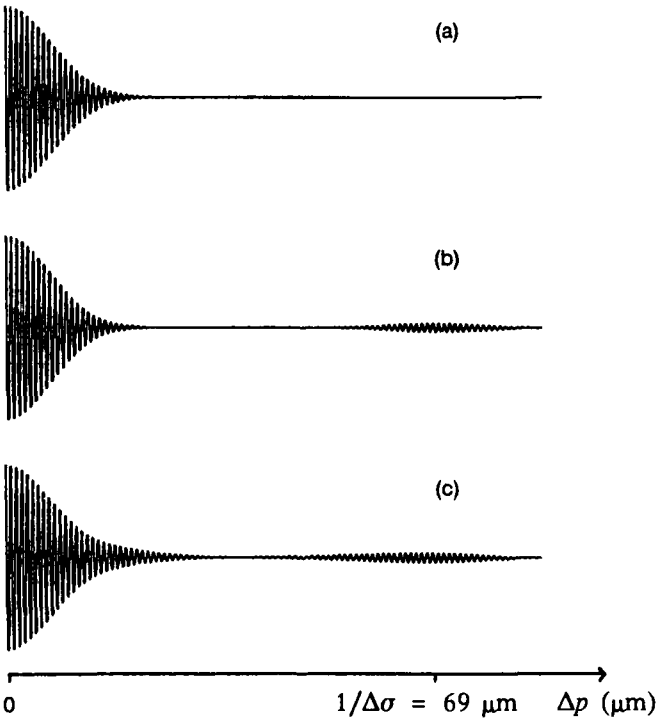

Figure 5. Source interferograms calculated for the source spectral distributions in figure 4.

EXPERIMENTAL CONFIGURATION

The properties of an interferogram, obtained from a Michelson interferometer using a partial coherence source, can be used to measure the thickness of a thin silicon CCD sample. Consider the schematic diagram of the experimental configuration in figure 6. The source is a commercially available edge-emitting, light-emitting diode (ELED), packaged in a hermetic housing, and coupled to a multimode fiber pigtail. The housing contains a thermoelectric cooler and a thermistor to stabilize the temperature and wavelength. The ELED emits in the wavelength region near 0.83 μm, with a spectral width of approximately 40 nm. The exact spectral energy distribution depends on temperature and operating current. Source distribution effects will be discussed in a subsequent section.

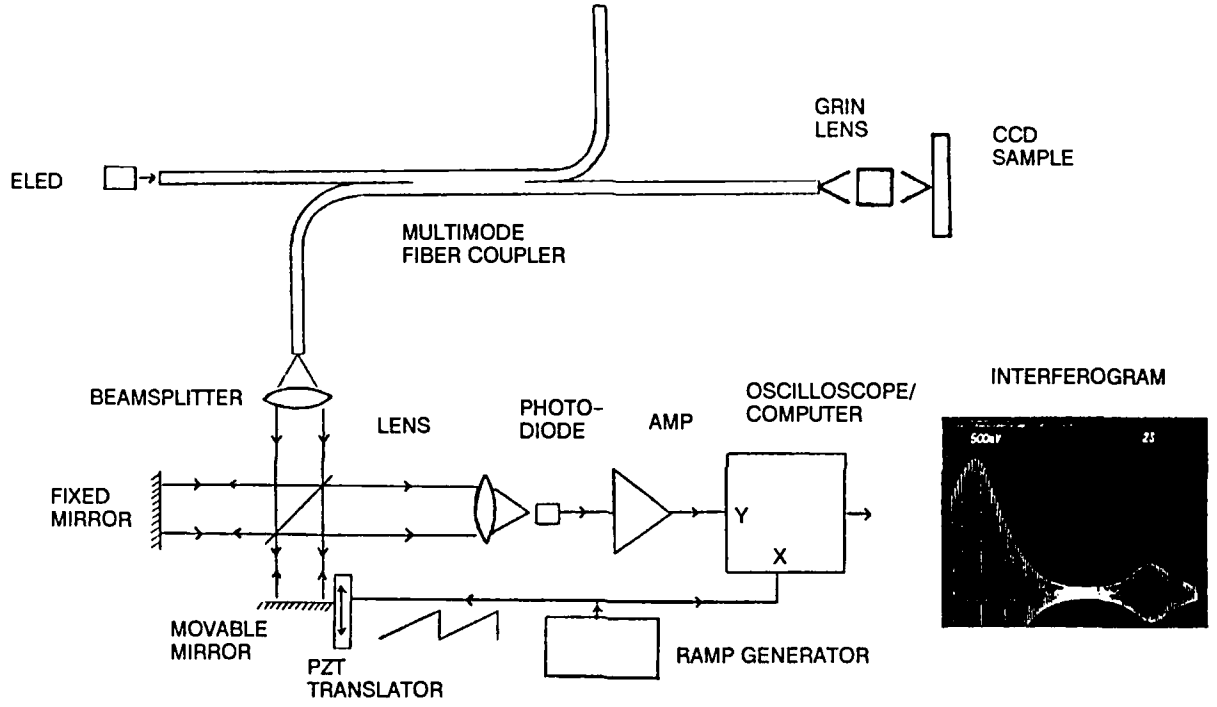

Figure 6. Experimental configuration for the measurement of CCD sample film thickness using an optical fiber coupler probe, a Michelson interferometer, and a partially coherent source.

The ELED fiber pigtail is spliced to one input port of a multimode-fused fiber bidirectional coupler. The coupler is a 3-dB (or 50/50) optical power splitter at 0.83 μm. One of the coupler output ports is positioned near a graded index (GRIN) rod lens where its output can be either collimated or focused onto the CCD sample to be evaluated. The second fiber output can serve as an input port for a visible wavelength (HeNe) laser used to align the interferometer portion of the measurement system, or it can be coupled to a spectrometer for monitoring the source spectral properties during a measurement.

The optical beam incident on a CCD sample of thickness, t, is partially reflected and transmitted at the first surface. The transmitted beam is again partially reflected at the back surface. The front- and back-surface-reflected beams are coupled back into the GRIN lens and the fiber coupler. Use of a multimode fiber maximizes the input/output coupling efficiency of the optical beams.[4,5] The fourth coupler port transmits the sample-reflected beams to the Michelson interferometer. The two waves are divided by the Michelson beamsplitter, and one set of wave packets is delayed with respect to the other by the variable path length difference, $2p_t$, between the two arms of the interferometer. This path-length difference is controlled by, and is proportional to, the voltage, V_p, applied to the linear piezoelectric transducer. The beams are recombined at the beamsplitter and interfere on the detector whose output current is proportional to the intensity of the interfering beams. This detector current is amplified and the amplifier voltage is either displayed on an oscilloscope as a function of V_p (i.e., p_t), or it can be converted to a digital signal and stored in a computer. A linear-ramp voltage is applied to the piezoelectric, and the fringe intensity versus displacement is recorded to produce the sample interferogram. The information in this interferogram enables one to determine the sample thickness, t.

MEASUREMENT METHODOLOGY

To understand how the thickness, t, of the sample is derived from the interferogram obtained from the reflected-sample beams, consider the wave packet diagram in figure 7, and the related

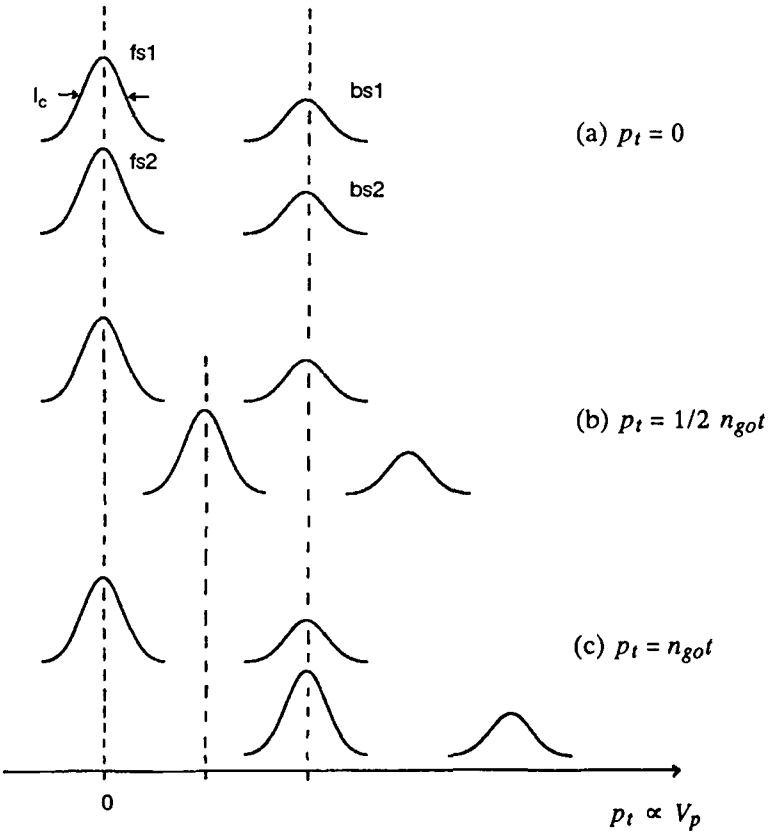

Figure 7. Relative delay of front-surface- and back-surface-reflected wave packets from sample by means of Michelson interferometer variable piezoelectric transducer displacement p_t.

computer-generated sample interferogram in figure 8. The reflected beams are represented by wave packets of width, l_c, separated by the optical-path-length difference $2n_{go}t$ between the front-surface-(*fs*) and back-surface-(*bs*) reflected beams.[1] Here, n_{go} is the group-refractive index of the sample material, in this case silicon, and has a value equal to 4.28 for λ_o = 0.83 μm.[2] For each of the three cases depicted, two sets of wave packets are shown, corresponding to the divided beams propagating in the two arms of the Michelson interferometer between the beamsplitter and the mirrors.

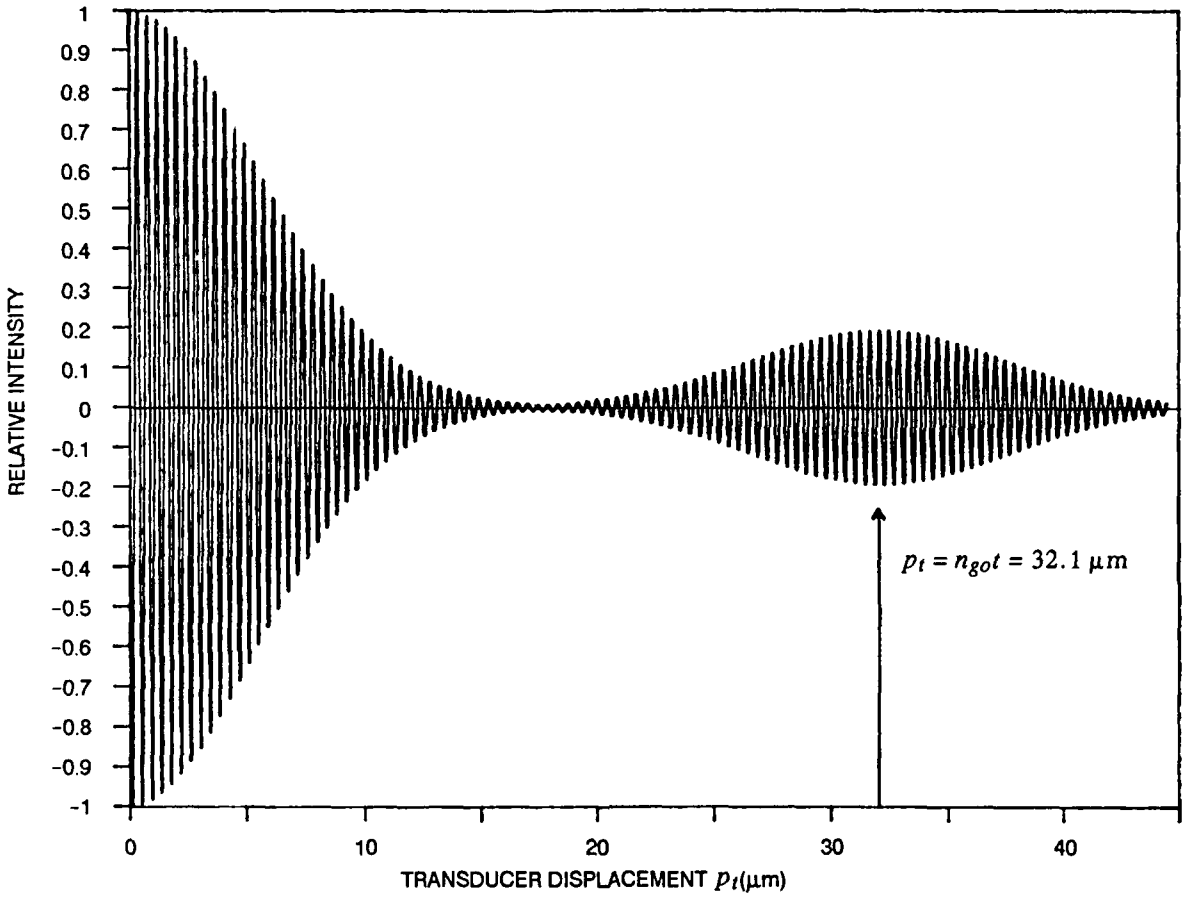

Figure 8. Computer-generated sample interferogram. Assumed values are λ_o = 0.83 μm, $\delta\lambda$ = 25 nm, and t = 7.5 μm.

As V_p is varied linearly from 0, one set of the reflected wave packets in the interferometer is proportionally delayed by an amount, $2p_t$, with respect to the other. At V_p = 0, the piezoelectric transducer displacement p_t = 0, and the wave packets are coincident in space so that they interfere coherently with maximum fringe visibility. As V_p is increased, the visibility decreases as a result of the reduced overlap of the wave packets. (The source-spectral width is assumed such that the coherence length is less than the optical-path difference between the front- and back-surface wave packets.) The visibility reaches a minimum near $p_t = 1/2\ n_{go}t$ where there is minimum overlap between the sets of wave packets. Then, the visibility increases as the first surface reflection in one arm overlaps the second surface reflection in the other arm. This overlap occurs at $p_t = n_{go}t$, where the *bs*-reflected

[1]The optical path difference between wave packets generated by a spectrally distributed source is proportional to the group index of refraction, not the phase index. For example, see appendix A and Hariharan, 1985.[6]

[2]This value for n_{go} can be calculated using the phase index values for various wavelengths found in Palik's Handbook of Optical Constant of Solids.[7]

beam in one arm and the *fs*-reflected beam in the other arm are coherent because of the compensation of the optical-path-length difference in the sample by the optical-path-length difference between the arms of the interferometer. Therefore, the difference in p_t, measured between the central maximum and the side peak in the interferogram envelope, corresponds to the optical thickness of the sample, $n_{go}t$. (The same result is obtained for the opposite direction of piezoelectric-transducer displacement, and a maximum of the interferogram envelope also occurs at $p_t = -n_{go}t$). Thus, a priori knowledge of the group index, together with the accurate measurement of p_t, allows for the determination of film thickness, t. A more rigorous mathematical derivation of the sample interferogram, including the effects of dispersion, is given in appendix A.

The transducer displacement, p_t, can be determined by accurate calibration of the displacement as a function of V_p, or by the method of fringe counting in the interferogram. Fringe-counting is based on the premise that each period or fringe within the envelope of the interferogram corresponds to a displacement of $\Delta p_t = \lambda_o/2$. Therefore, if sufficient visibility exists over the range of p_t from 0 to $n_{go}t$, the number, N, of fringes between the central peak and one of the side peaks can be counted to determine t by

$$n_{go}t = N\lambda_o/2 \quad or \quad t = N\lambda_o/2n_{go} \tag{7}$$

For the example shown in figure 8, the source was assumed to have a symmetric pure Gaussian spectral distribution of width $\delta\lambda = 25$ nm, centered about $\lambda_o = 830$ μm, and the sample thickness is $t = 7.5$ μm. Counting the number of fringes between the central maximum and the secondary maximum yields $N = 77$, which from the above relation gives $t = 7.47$ μm, in good agreement with the assumed value. Note that the uncertainty in determining the location of the secondary maximum is no greater than one fringe, which corresponds to an uncertainty in t of $1/N$ or, in this case 1.3 percent.

Again, note that the mean wavelength of the source distribution must be accurately known in order to calculate t. This can be done by simultaneously measuring the source-spectral distribution via the unused coupler port interfaced to a spectrometer during the recording of the sample interferogram.

In a practical measurement system, control of the scanning-piezoelectric voltage, spectral distribution measurement, recording of the interferogram, determination of the envelope peaks, and calculation of the sample thickness, would all be done using an automated computer control and data analysis system. Such a system was not used in this work, but its implementation would be straightforward.

Fringe-counting is an accurate means by which the thickness of thin samples can be measured. For samples with thickness so large that the optical path in the sample is many times greater than the coherence length of the source, the fringe visibility will be negligible in the region between the central and secondary maxima. Determining the occurrence of a fringe peak is not possible. In the case of large t values, a supplementary method must be used. In this regime, the accuracy need not be on the order of a fringe, since it is only the final etched-sample thickness that must be known with high accuracy. One means to measure large values of t, is to mount one of the Michelson interferometer mirrors on a translation stage driven by a stepping motor. The stepping motor output can easily be controlled and monitored to provide path-length-measurement accuracies of 10 μm over a wide range of translation. During the initial stages of sample etching, where the thickness is on the order of 1 mm, the stepping motor would be used to traverse the Michelson mirror over the distances necessary to cause the *fs* and *bs* wave packets to overlap. Then, in the final stages of etching, where the thickness is small (approximately 10 μm), the more accurate piezoelectric transducer and the fringe-counting method would be used.

EXPERIMENTAL RESULTS

Interferograms were made for various thin silicon CCD samples with a nominal thickness of 8 μm. The ELED temperature and current were held constant at 25°C and 10 mA. The source spectral distribution under these conditions is shown in figure 9. The mean wavelength is $\lambda_o = 0.847$ μm, and the spectral width is approximately $\delta\lambda \simeq 20$ nm or $\delta\sigma \simeq 0.028\,\mu m^{-1}$. Some periodic structure and asymmetry are also present, but these effects proved to be inconsequential as discussed in the following section.

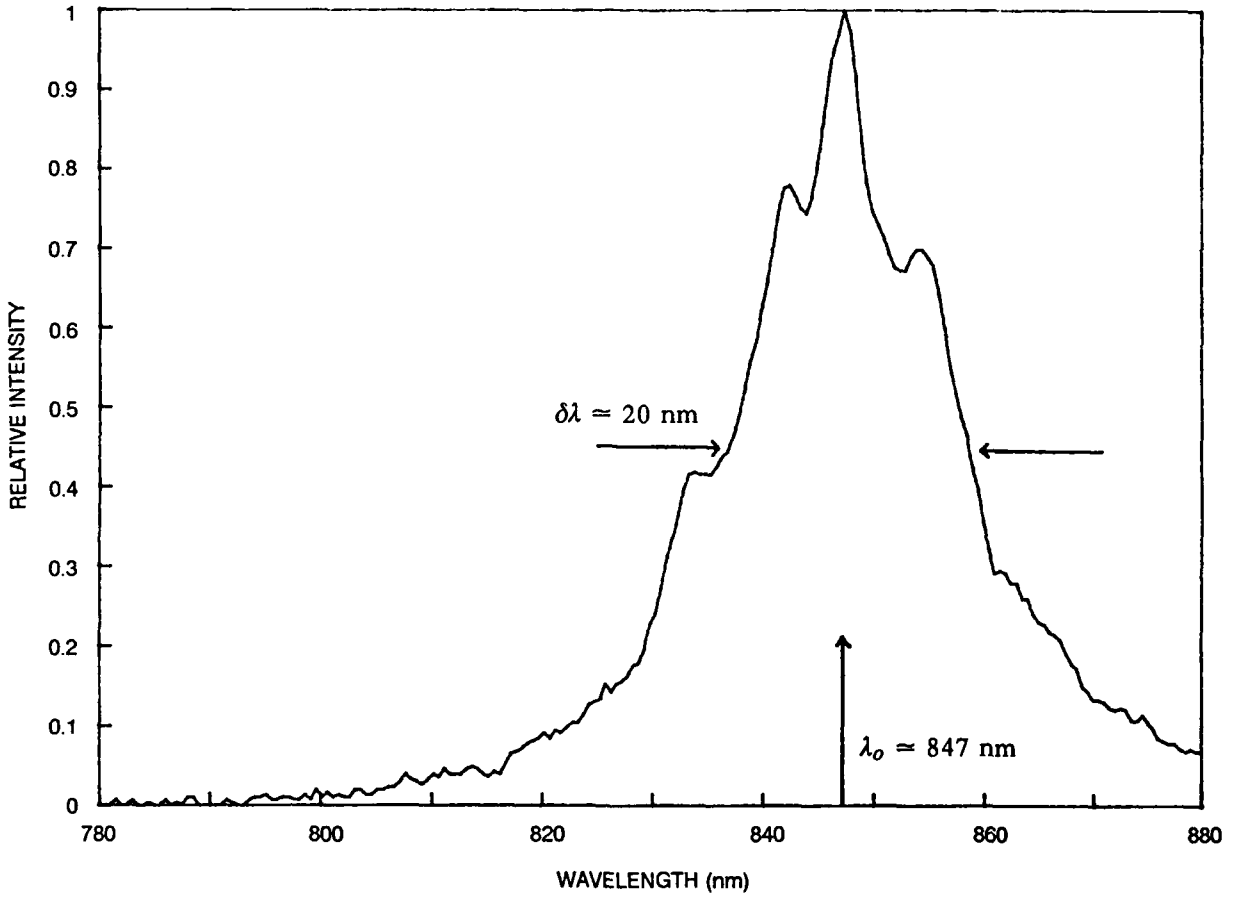

Figure 9. Spectral distribution for ELED used in the experiments operating at 10 mA. Mean wavelength is 847 nm and spectral width is approximately 20 nm.

The output beam of the fiber coupler was focused onto a small region, about 100 μm in diameter, at the center of the sample. The center was found by displacing the sample along orthogonal axes in a plane normal to the beam and locating the positions of the sample edges by monitoring the intensity of the reflected beam.

A typical interferogram, obtained by photographing the oscilloscope trace of the detector-amplifier voltage, V_d, versus the transducer-drive voltage, V_p, is shown in figure 10. In this photograph, the number of fringes can be counted visually to yield $N = 79$, which, using equation (7), corresponds to a sample thickness of 7.8 μm at the center. Numerous silicon CCD samples were measured and the results are tabulated in table 1.

An attempt was made to determine if any variation of sample thickness exists as a function of position on the sample. Again, the edges of the 2 mm × 2 mm sample were located and a matrix of points, equally spaced at 500 μm intervals within this area, was probed by the output beam of the coupler. The results for one particular sample are shown in table 2, which shows that the maximum variation of thickness over the sample is 0.3 μm.

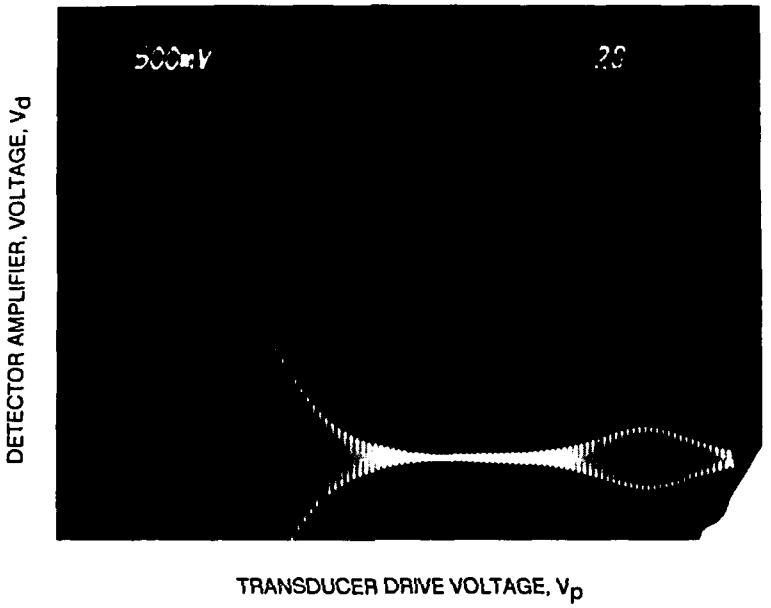

Figure 10. Actual sample interferogram obtained by photographing oscilloscope recording of detector-amplifier-output voltage versus piezoelectric-transducer-ramp voltage. Number of fringes from central maximum to secondary maximum is N = 79, corresponding to a sample thickness of t = 7.8 μm.

Table 1. Results of sample thickness measurement.

Hughes CCD Sample #	N	t (μm)
7153AA20R1-6F	87	8.6
7154AA19R1-6J	78	7.7
7153AA20R1-5J	86	8.5
7154AA5R1-4D	77	7.6
7154AA3R1-5E	84	8.3
7154AA5R1-5A	80	7.9
7153AA09R2-7C	76	7.5
7153AA09R2-4G	81	8.0
7153AA14R1-2C	77	7.6
7153AA14R1-2J	79	7.8
7154AA3R1-6A	84	8.3

Table 2. *Sample thickness variation with position.*

		x (μm)		
		-500	0	+500
y (μm)	+500	7.7	7.9	7.7
	0	7.6	7.8	7.8
	-500	7.7	7.6	7.6

DISCUSSION AND CONCLUSIONS

A method has been described for the precision measurement of thin silicon CCD samples using a fiber-optic-coupler probe, an edge-emitting LED (ELED), and a Michelson interferometer. The measurement precision is one optical fringe, or about 0.1 μm. The fiber-optic probe can do remote in situ measurements and variable position, localized thickness measurements. The flexibility of the fiber, and the small size and chemical inertness of the fiber/GRIN rod lens assembly, enable the probe end to be configured in a probe housing that could be placed close to the sample within the etching chamber while the sample is processed. In this way, continuous sample-thickness measurements could be made, and the data used to control the etching parameters.

While the basic operation of the equipment and measurement methods have been successfully demonstrated, several limitations and potential future modifications need to be considered. As mentioned previously, the spectral distribution of the source determines several basic features of the sample interferogram. The source width (hence, the coherence length) must be such that the fringe visibility goes through a distinct minimum, while maintaining adequate visibility for fringe-counting, as the Michelson interferometer is scanned to generate the interferogram. For samples with thickness values on the order of 5 to 10 μm, the source must be either an ELED or a superluminescent diode (SLD). A suitable SLD was not available for this work, and therefore the system could not be evaluated with this type of source. (The SLD offers potentially higher optical powers than the ELED, which could be important in certain applications, such as in situ measurements, where the optical power of the reflected sample beam might be small.)

Either type of source can exhibit both spectral structure and asymmetry. It is important that the structure be minimized so that the source interferogram components do not interfere with the sample interferogram secondary maximum. In this work, the ELED source spectral properties were carefully investigated. Source spectra measured at a constant temperature of 25°C for various drive currents are shown in figure 11. Note that there is significant source structure and asymmetry for the higher operating currents, and that the mean wavelength shifts to higher values as the current is decreased. To minimize the effects of source spectrum periodic structure and asymmetry discussed in the previous sections, the ELED was operated at a current of 10 mA. (Even at this low-operating current there was adequate light energy to provide a large signal-to-noise ratio (SNR) for the system detector output.) Figure 9 is an expanded plot of the spectral distribution for an operating current of 10 mA. It can be seen that even at this low-operating current some structure is present with a period of $\Delta\lambda = 5.4\ nm$ ($\Delta\sigma = 0.0075\ \mu m^{-1}$).

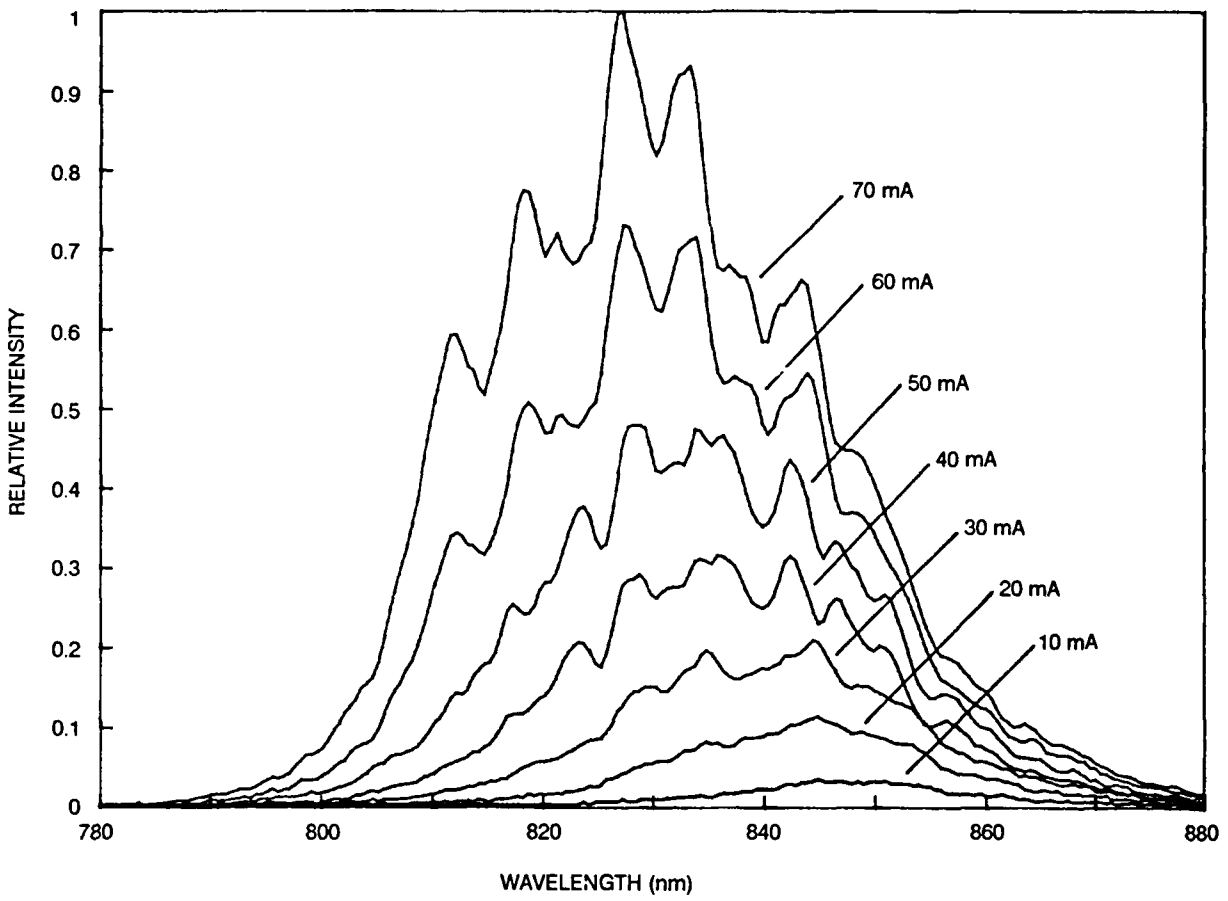

Figure 11. ELED source spectra at 25°C for various operating currents. Presence of structure and asymmetry increase as current increases, while mean wavelength shifts to smaller values.

The effect of this structure is minimal in the measurement of thin silicon films. First, the period is such that a contribution to the source interferogram would be made at a path difference of $\Delta p = 1/\Delta\sigma = 133$ μm, which is much greater than the sample round-trip optical-path length of $2n_{got} \simeq 60$ μm. Second, the amplitude of the periodic structure is much less than the Gaussian component amplitude and, therefore, its contribution to the interferogram will be correspondingly small. These conclusions are confirmed by the 10-mA source interferogram shown in figure 12 for a range of Δp from -10 μm to 110 μm.

The mean wavelength must also be considered in the selection of an appropriate optical source and depends on its material composition. Both GaAlAs and InGaAsP ELEDs, operating in the spectral regions near 0.83 μm and 1.3 μm, respectfully, are commercially available.

Each fringe in the interferogram corresponds to an optical-path difference of $\lambda_o/2$, and, therefore, the shorter the wavelength, the greater the precision in the measurement of the sample thickness. In this respect, the GaAlAs source with $\lambda_o \simeq 0.83$ μm would be better than an InGaAsP source. On the other hand, the absorption of light is greater in silicon for shorter wavelengths, and, therefore, for relatively thick samples, the back-surface-reflected beam would be too strongly attenuated to contribute to the interferogram.

The value of the interferogram secondary maximum, relative to the maximum at 0 path-length difference, is related to the ratio of the fields resulting from the back- and front-surface reflections. A

ratio of 10 percent is, somewhat arbitrarily, chosen as the minimum value that will result in a clearly discernible secondary maximum for fringe-counting.

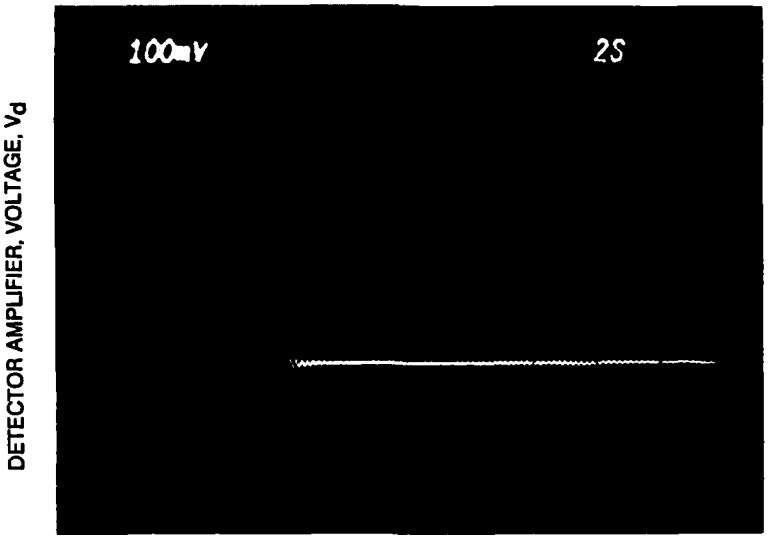

Figure 12. Source interferogram for ELED operating at 10 mA. Minimal periodic structure is indicated by lack of significant interferogram amplitude other than central envelope.

The back-surface field is reduced with respect to the first surface field by three factors in addition to the sample absorption. First, the coupling of the reflected beams back into the fiber will be different due to the unequal distances from the principal plane of the GRIN rod lens. (In practice, the relative position of the lens and the sample is adjusted so that the height of the secondary maximum is maximized for a given film thickness.) Second, the back-surface reflection is transmitted twice through the sample/air-first surface, and, therefore, the back-surface-field amplitude is reduced by a factor of t^2 relative to the front-surface field. Here, t is the coefficient of the electric field transmission, and for silicon in $t^2 \simeq 0.68$. Third, while the front surface interface is with air, the back surface has on it the CCD circuitry, which consists of thin layers of polymers, metals, and oxides. These materials are not necessarily uniform, nor highly reflecting, with the result that the back-surface reflection is less than the front-surface silicon/air reflection. The reduction of the back-surface reflection due to these factors, and the absorption by the material itself, determine the source wavelength limitations on the sample thickness that can be measured.

If the coupling efficiency back into the fiber is assumed to be equal for the front- and back-surface-sample-reflected beams, that the reflection coefficients are equal for the two surfaces, and taking into account the reduction in the back-surface field by the interface transmittance factor, t^2, then a limit on the maximum thickness of the sample can be determined due to absorption. The ratio of the interferogram envelope secondary and primary maxima is

$$E_{fs}E_{bs}/(E_{fs}^2 + E_{bs}^2) \tag{8}$$

where

$$E_{bs}/E_{fs} = t^2 \exp(-\alpha t) \tag{9}$$

and $\alpha \simeq$ is the absorption coefficient of silicon. For $\lambda = 0.83$ μm, $\alpha \simeq 700$ cm^{-1}, while for $\lambda = 1.3$ μm silicon is transparent ($\alpha \rightarrow 0$).[8] Equations (8) and (9) can be used to calculate the maximum sample thickness that would yield a secondary interferogram envelope maximum equal to 10 percent of the primary maximum. The result is $t_{max} \simeq 27$ μm for $\lambda = 0.83$ μm.

Note that in figure 10, the ratio of the interferogram maxima for a 7.6 μm sample is approximately 10 percent. This is an indication that the assumptions regarding beam-to-fiber coupling efficiencies and equal-interface-reflection coefficients are not necessarily valid. In practice, for a sample thickness greater than 10 μm, the ratio will always be less than 10 percent at 0.83 μm due to increased absorption; therefore, the longer wavelength InGaAsP source would be more suitable.

REFERENCES

1. Fowles, G. R. 1975. *Introduction to Modern Optics, second edition*. p. 73. Holt, Rinehart and Winston, Inc., New York.

2. Hopkins, H. H. 1967. "Theory of Coherence." p. 232. in *Advanced Optical Techniques*, Van Heel, A.C.S., editor, John Wiley & Sons, Inc., New York.

3. Cathey, W. T. 1974. *Optical Information Processing*. p. 78. John Wiley & Sons, New York.

4. Bosselmann, T. H. and R. Ulrich. Sep 1984. "High Accuracy Position Sensing with Fiber Coupled White Light Interferometers," in *Proc. Second Int. Conf. Optical Fiber Sensors*, Stuttgart, FRG. pp. 361-364.

5. Takada, K. Jul 1987. "Trench Depth Measurement System for VLSI DRAM's Capacitor Cells Using Optical Fiber and Michelson Interferometer," *J. Lightwave Technology*, vol. LT-5, no. 7, pp. 881-887.

6. Hariharan, P. 1985. *Optical Interferometry*. p. 33. Academic Press, Inc., New York.

7. Palik, E. D. 1985. *Handbook of Optical Constants of Solids*. pp. 547-569. Academic Press, Inc., New York.

8. Sze, S. M. 1969. *Physics of Semiconductor Devices*. p. 661. Wiley-Interscience, New York.

GLOSSARY OF SYMBOLS AND ABBREVIATIONS

bs	back surface
CCD	charge-coupled device
$E(\sigma)$	interferometer-output-optical field
$E_S(\sigma)$	source-optical field
E_{fs}	optical field from sample-front surface
E_{bs}	optical field from sample-back surface
ELED	edge-emitting, light-emitting diode
fs	front surface
GRIN	graded index
HeNe	Helium Neon (laser)
l_c	source-coherence length
LED	light-emitting diode
mA	milliampere
n	phase index of refraction of the sample material
n_g	group index of refraction of the sample material
n_{go}	group index of refraction of the sample material at $\sigma = \sigma_o$
n_O	phase index of sample material for $\sigma = \sigma_o$
n_O'	derivative of phase index for $\sigma = \sigma_o$
N	number of interferogram fringes between primary and secondary maxima
nm	nanometer
μm	micrometer
p_1	optical path length of (first) wave packet
p_2	optical path length of (second) wave packet
p_t	differential length between the interferometer arms
SLD	superluminiscent diode
SNR	signal-to-noise ratio

t	thickness of the sample to be measured
t	optical field transmittance at sample/air interface
V_d	photodetector output voltage
V_p	voltage applied to interferometer transducer
α	absorption coefficient of silicon
$\delta\sigma$	width of spectral energy distribution in wavenumbers
$\delta\lambda$	spectral width of source in wavelength units (nm or μm)
Δp	path-length difference between optical wave packets
$\Delta\lambda$	period of spectral structure in wavelength units
$\Delta\sigma$	period of spectral structure in wavenumber units
λ	wavelength of optical field (nm or μm)
λ_o	mean wavelength of source distribution
σ	wavenumber of optical field (μm^{-1})
σ_o	mean wavenumber of source distribution

APPENDIX A

THEORETICAL DERIVATION OF THE INTERFEROGRAM FOR A SYMMETRIC MICHELSON INTERFEROMETER WITH A TWO-BEAM INPUT FROM A DISPERSIVE MEDIUM

In this appendix, a more detailed derivation of the sample interferogram is presented. Again the interferometer is a symmetric Michelson interferometer with a two-beam input from the sample; but now, the effects of material dispersion are included. As in the previous treatment of the source interferogram, the inputs to the interferometer are assumed to have the same polarization, can be treated as emanating from point sources, and the beams have no angular misalignment. The use of the fiber coupler input assures that all of these assumptions are valid.

It will be shown that for a typical sample thickness of the order of 10 μm, the effects of material dispersion can be neglected, and that the previous results regarding the features of the sample interferogram, which were based on the less qualitative wave-packet overlap treatment, are completely valid.

Referring to figure 6, the continuous optical output field from the source, represented by $E_s(\sigma)$, is incident on the sample via the bidirectional coupler. This beam is partially reflected from the front and back surfaces with a relative phase difference between the reflected fields of $4\pi\sigma nt$, corresponding to the optical-path length in the material. Here n is the phase index of the material evaluated at the particular wavenumber σ. Due to the partial transmittance of the optical field at the sample material boundaries, the amplitude of the back-surface-reflected beam relative to the front-surface reflection is t^2, where t is the transmittance of the sample/air interface. The front- and back-surface-reflected beams are coupled into the Michelson interferometer via the GRIN rod lens and the fiber coupler. The differential optical-path length between the two arms of the interferometer is $2p_t$, and is varied by means of the piezoelectric transducer.

Using the complex field notation, and omitting the explicit time dependence of the fields, the output field from the interferometer is expressed as

$$E(\sigma) = Re\{U(\sigma)\} \tag{A-1}$$

where $U\{\sigma\}$ is the complex field amplitude as a function of σ,

$$\begin{aligned} U(\sigma) &= E_s(\sigma)[1 + \exp(i4\pi\sigma p_t)][1 + t^2\exp(i4\pi\sigma nt)] \\ &= E_s(\sigma)[1 + t^2\exp(i4\pi\sigma nt) + \exp(i4\pi\sigma p_t) + t^2\exp(i4\pi\sigma p_t + nt)] \\ &= U_1 + U_t + U_p + U_2 \end{aligned} \tag{A-2}$$

(Note that $U_1 = E_s(\sigma)$, and that common phase and amplitude factors have been omitted.)

In this expression, it is understood that n is, in general, a function of σ. Also, it has been assumed that the mirror reflectances are both equal to 1, and that the beamsplitter is lossless. The time-averaged intensity for a wavenumber component σ is then expressed as

$$
\begin{aligned}
I(\sigma) &= |U(\sigma)|^2 = UU^* \\
&= |U_1|^2 + |U_t|^2 + |U_p|^2 + |U_2|^2 + (U_1U_t^* + U_1^* U_t) + (U_pU_2^* + U_p^* U_2) \\
&+ (U_1U_p^* + U_1^* U_p) + (U_tU_2^* + U_t^* U_2) \\
&+ (U_1U_2^* + U_1^* U_2) + (U_tU_p^* + U_t^* U_p
\end{aligned}
\tag{A-3}
$$

In the above equation, the terms have been grouped according to the constant terms on the first line, which are not a function of p_t, and the remainder of the terms, which are variable. This expression can be further simplified by using the relation $(Z+Z^*) = 2Re\{Z\}$, where Z is any complex number, and by noting that

$$|U_1|^2 = |U_p|^2 = |E_s(\sigma)|^2$$

$$|U_t|^2 = |U_2|^2 = t^2|E_s(\sigma)|^2$$

$$(U_pU_2^* + U_p^* U_2) = U_1U_t^* + U_1^* U_t$$

and $$(U_tU_2^* + U_t^* U_2) = t^2(U_2U_p^* + U_1^* U_p)$$

Using these relations,

$$I(\sigma) = 2[(1+t^2)|E_s(\sigma)|^2 + 2\ Re\{U_1U_t\} + (1+t^2)\ Re\{U_1U_p\} + Re\{U_1U_2\} + Re\{U_tU_p^*] \tag{A-4}$$

The first three terms are constants with respect to p_t, and contribute to the constant intensity present in the output. The last three terms contain the information related to the sample thickness t.

The total intensity $I(p_t)$ of the output beam is obtained by integrating the function $I(\sigma)$ over the entire spectral range of the source,

$$I(p_t) = \int I(\sigma)d\sigma$$

Denoting the integrals of the three constant terms in the expression for $I(\sigma)$ as $I(\infty)$, the expression for $I(p_t)$ becomes

$$I(p_t) = I(\infty) + 2\ Re\left\{(1+t^2)\int_{\infty}^{\infty} U_1U_p d\sigma + \int_{\infty}^{\infty} U_1U_2 d\sigma + \int_{\infty}^{\infty} U_tU_p^*\, d\sigma\right\} \tag{A-5}$$

Because of the limited spectral range of the source, the limits of integration have been chosen to be $\pm\ \infty$ for mathematical convenience. The notation for $I(\infty)$ follows by recognizing that as $p_t \rightarrow \infty$, the three nonconstant terms $\rightarrow 0$, and therefore, the first three terms simply represent the value of $I(p_t)$ at $p_t \rightarrow \infty$.

At this point, a specific functional form for the source energy spectral distribution, $|E_s(\sigma)|^2$, is chosen which represents typical high-radiance-limited-spectral width sources, such as light-emitting diodes (LEDs) and superluminescent diodes (SLDs). These sources can be represented by a normalized Gaussian spectral distribution of the form

$$|E_t(\sigma)|^2 = (1/\delta\sigma)\exp\{-\pi(\sigma-\sigma_o)^2/(\delta\sigma)^2\}\ . \tag{A-6}$$

To evaluate the integrals in equation (A-5), a change of variables is made so that the integrals are symmetric about σ_o. Letting $s = \sigma - \sigma_o$, and setting the limits of integration on s to be $\pm \infty$ (this is valid since $\sigma_o >> \delta\sigma$), each of the three integrals in equation (A-5) can be put in a standard form that can be found in integral tables. The general relation from reference 1 is

$$\int_{-\infty}^{+\infty} \exp\{-[as^2 + 2bs + c]ds = (\pi/a)^{\frac{1}{2}} \exp\{(b^2 - ac)/a\} . \tag{A-7}$$

Here, a and b are the appropriate constants for each integral. Using equations (A-5), (A-6), and (A-7), the total intensity is then

$$\begin{aligned} I(p_t) = I(\infty) + 2\,Re\Bigg(& (1 + t^2)\exp[i4\pi\sigma_o p_t]\exp[-\pi(p_t)^2(2\delta\sigma)^2] \\ & + \frac{2t^2\exp[i4\pi\sigma_o(p_t + n_o t)]}{[1 - in_o' t(2\delta\sigma)^2]^{\frac{1}{2}}}\exp\{-\pi(p_t + n_{go}t)^2(2\delta\sigma)^2/[1 - in_o' t(2\delta\sigma)^2]\} \\ & + \frac{2t^2\exp[-i4\pi\sigma_o(p_t - n_o t]}{[1 - in_o' t(2\delta\sigma)^2]^{\frac{1}{2}}}\exp\{-\pi(p_t - n_{go}t)^2(2\delta\sigma)^2/[1 - in_o' t(2\delta\sigma)^2]\}\Bigg) . \end{aligned} \tag{A-8}$$

To obtain this result, it has been assumed that the phase index of refraction, which is a function of the wavenumber, can be expanded in a Taylor series near σ_o,

$$\begin{aligned} n = n(\sigma) &= n(\sigma_o) + (\sigma - \sigma_o)(dn/d\sigma)|_{\sigma_o} \\ &\equiv n_o + (\sigma - \sigma_o)n_o' . \end{aligned}$$

Also, the notation n_{go} has been used for the value of the group index at $\sigma = \sigma_o$.

$$n_{go} = n_g(\sigma)|_{\sigma_o} = [n(\sigma) + \sigma(dn/d\sigma)]|_{\sigma_o} .$$

Using equation (A-8), the features of the interferogram, which were derived previously using the wave packet overlap analysis, are confirmed. First, the interferogram function is an oscillatory function with an envelope that consists of three Gaussian functions centered at $p_t = 0$ and $\pm n_{go}t$. Also, the shape of the envelope function, and the phase of the oscillation, depend on the source mean wavenumber and spectral width, the sample thickness, and the phase and group refractive indices of the sample.

To this point, the derivation of the interferogram function is valid for a dispersive sample medium of any thickness. The contribution of dispersion appears whenever the factor n_o' is present, and the magnitude of the effect increases with increasing sample thickness. It can be seen that dispersion affects both the phase and amplitude of the interferogram function. The amplitude reduction of the

secondary maxima is not significant as long as there is sufficient signal to allow for peak height determination for fringe-counting. The phase is affected by both the addition of constant phase terms, and by a chirping, or nonlinear variation of phase with p_t.

To assess the effect of dispersion, it is helpful to consider the magnitude of these factors for a particular experimental situation corresponding to a practical sample measurement. The source used in these experiments was chosen to be an ELED with a mean wavelength of approximately 0.85 μm and a spectral width of approximately 20 nm (see figure 9). These values correspond to values of $\sigma_o = 1.18\,\mu m^{-1}$ and $\delta\sigma = 0.028\ \mu m^{-1}$. The sample is a silicon CCD with a thickness on the order of 10 μm. The values of the group index and the derivative of the phase index at p_t can be derived from published data in reference 7, and are found to be $n_{go} = 4.28$ and $n_o' = 0.5$ μm.

For these values of p_t, $\delta\sigma$, t and n_o' it is found that the contributions to the interferogram due to material dispersion can be neglected. For example, the constant phase factor is

$$\phi = \tan^{-1}(2n_o' t(\delta\sigma)^2) = \tan^{-1}(0.008) = 0.008 \text{ rad}$$

Similar negligible values are obtained for the amplitude reduction factor and the chirp phase term.

It should be noted that these negligible values are for small values of t, and that for larger values, these effects should be included. For example, if the maximum tolerable phase offset due to material dispersion is chosen to be 10 percent for either the second or third terms in the interferogram, then the corresponding maximum sample thickness is $\simeq$ 50 μm.

If the sample thickness is small enough that the material dispersion effects can be ignored, then the interferogram function can be simplified to give (omitting the t dependent amplitude factors)

$$\begin{aligned} I(p_t) = I(\infty) &+ \cos\{4\pi\sigma_o p_t\}\ \exp[-\pi(p_t)^2(\delta\sigma)^2] \\ &+ \cos\{4\pi\sigma_o(p_t + n_o t)\}\ \exp[-\pi(p_t + n_{go}t)^2(2\delta\sigma)^2] \\ &+ \cos\{4\pi\sigma_o(p_t - n_o t)\}\ \exp[-\pi(p_t - n_{go}t)^2(2\delta\sigma)^2] \end{aligned} \qquad \text{(A-9)}$$

Equation (A-9) is the mathematical representation of the result that was derived qualitatively using the wave packet approach, and which is represented by the interferogram shown in figure 8.

REFERENCE

1. Abramowitz, M. and I. A. Stegun. 1965. *Handbook of Mathematical Functions*. p. 303. Dover Publications Inc., New York.

REPORT DOCUMENTATION PAGE

Form Approved
OMB No. 0704-0188

1. AGENCY USE ONLY *(Leave blank)*	2. REPORT DATE	3. REPORT TYPE AND DATES COVERED
	February 1991	Final: Oct 1988 - Sep 1989

4. TITLE AND SUBTITLE

THICKNESS MEASUREMENTS OF SILICON FILMS USING PARTIAL COHERENCE INTERFEROMETRY

5. FUNDING NUMBERS

PE: WPN
PROJ: 55-WM06
SUBPROJ: X0951
ACC: DN687536

6. AUTHOR(S)

M. N. McLandrich and D. J. Albares

7. PERFORMING ORGANIZATION NAME(S) AND ADDRESS(ES)

Naval Ocean Systems Center
San Diego, CA 92152–5000

8. PERFORMING ORGANIZATION REPORT NUMBER

NOSC TR 1372

9. SPONSORING/MONITORING AGENCY NAME(S) AND ADDRESS(ES)

Strategic Systems Project Office
Washington, DC 20360 (SSPO-SP273)

10. SPONSORING/MONITORING AGENCY REPORT NUMBER

11. SUPPLEMENTARY NOTES

12a. DISTRIBUTION/AVAILABILITY STATEMENT

Approved for public release; distribution is unlimited.

12b. DISTRIBUTION CODE

13. ABSTRACT *(Maximum 200 words)*

An optical system composed of a Michelson interferometer, a short coherence length edge-emitting, light-emitting diode (ELED), and a fiber-optic-coupler probe has been described and used to measure the thickness of thin silicon charge-coupled device (CCD) films. The measurement precision for samples with a thickness of the order of 10 μm is better than 0.1 μm, and the range of thickness that can be measured can be from a few micrometers to hundreds of micrometers if a suitable source is used. The fiber probe assembly is adaptable for remote in situ measurements of samples within an etching chamber, and the measurement results can be used to control the sample etching process. The fiber probe also allows for localized measurements at selected positions across the area of the sample, and these results can be used for control of thickness uniformity.

14. SUBJECT TERMS

charge-coupled device (CCD), etching process, substrate thickness, microcircuitry, interferometry, superluminescent diode (SLD), edge-emitting light-emitting diode (ELED)

15. NUMBER OF PAGES

30

16. PRICE CODE

17. SECURITY CLASSIFICATION OF REPORT	18. SECURITY CLASSIFICATION OF THIS PAGE	19. SECURITY CLASSIFICATION OF ABSTRACT	20. LIMITATION OF ABSTRACT
UNCLASSIFIED	UNCLASSIFIED	UNCLASSIFIED	SAME AS REPORT

INITIAL DISTRIBUTION

Code 0012	Patent Counsel	(1)
Code 534H	N. T. Kamikawa	(1)
Code 534H	A. T. Nakagawa	(1)
Code 55	H. E. Rast	(1)
Code 551	G. L. Haviland	(1)
Code 553	G. A. Garcia	(1)
Code 553	D. J. Albares	(10)
Code 554	E. P. Kelley	(1)
Code 562	M. N. McLandrich	(10)
Code 714	K. E. Rogers	(1)
Code 82	R. J. Kochanski	(1)
Code 936	R. A. Gamble	(1)
Code 946	S. J. Cowen	(1)
Code 952B	J. Puleo	(1)
Code 961	Archive/Stock	(6)
Code 964B	Library	(3)

Defense Technical Information Center
Alexandria, VA 22304-6145 (4)

NOSC Liaison Office
Washington, DC 20363-5100 (1)

Center for Naval Analyses
Alexandria, VA 22302-0268 (1)

DARPA
Arlington, VA 22209 (1)

Strategic Programs Office
Crystal City
Washington, DC 20362 (1)